Journal of Magnetic Resonance **140,** 120–130 (1999)
Article ID jmre.1999.1835, available online at http://www.idealibrary.com on IDEAL®

Time-Domain Quantification of Series of Biomedical Magnetic Resonance Spectroscopy Signals

Leentje Vanhamme,* Sabine Van Huffel,* Paul Van Hecke,† and Dirk van Ormondt‡

*Department of Electrical Engineering (ESAT), Katholieke Universiteit Leuven, Kard. Mercierlaan 94, 3001 Leuven, Belgium;
†Biomedical NMR Unit, Katholieke Universiteit Leuven, Gasthuisberg, 3000 Leuven, Belgium; and
‡Department of Applied Physics, University of Technology of Delft, The Netherlands

Received October 21, 1998

Quantification of individual magnetic resonance spectroscopy (MRS) signals is possible in the time domain using interactive nonlinear least-squares fitting methods which provide maximum likelihood parameter estimates under certain assumptions or using fully automatic, but statistically suboptimal, black-box methods. In kinetic experiments time series of consecutive MRS spectra are measured in which information concerning the time evolution of some of the signal parameters is often present. The purpose of this paper is to show how AMARES, a representative example of the interactive methods, can be extended to the simultaneous processing of all spectra in the time series using the common information present in the spectra. We show that this approach yields statistically better results than processing the individual signals separately.

Key Words: **MRS data quantification; AMARES; time series; SVD; nonlinear least squares.**

INTRODUCTION

In biochemical studies magnetic resonance spectroscopy (MRS) signals are often acquired consecutively to monitor metabolic changes over time. If some of the parameters of these spectra are related, it is advantageous to process the signals of the time series simultaneously taking these relations into account. In this paper we address how to extend a typical time-domain quantification method to the simultaneous processing of a series of MRS signals.

In many practical situations, the measured data points y_n of a MRS signal can be modeled as a sum of exponentially damped complex-valued sinusoids (also called Lorentzians):

$$y_n = \bar{y}_n + e_n = \sum_{k=1}^{K} a_k e^{j\phi_k} e^{(-d_k + j2\pi f_k)t_n} + e_n$$
$$n = 0, 1, \ldots, N-1, \qquad [1]$$

where $j = \sqrt{-1}$, a_k is the amplitude, ϕ_k the phase, d_k the damping, and f_k the frequency of the kth sinusoid ($k = 1, \ldots, K$); $t_n = n\Delta t + t_0$ with Δt the sampling interval, t_0 the time between the effective time origin and the first data point to be included in the analysis, and e_n complex white Gaussian noise. The bar on y indicates that this quantity represents the model function rather than the actual measurements. The amplitudes are proportional to the amount of each metabolite present and need to be determined as accurately as possible. Other types of model functions, like Gauss or Voigt, are also sometimes used to model the measured data. Typical of this application is the presence of prior knowledge derived from biochemistry, spin properties, or *in vitro* studies. This biochemical prior knowledge can normally be expressed as a set of linear relations between parameters of the same type.

To extract the parameters from a MRS signal, interactive time-domain methods exist that are iterative, require user involvement, allow the inclusion of prior knowledge, and have no restrictions on the type of model function used. The algorithms minimize the difference between the nonlinear model function and the data. This approach leads to maximum likelihood (ML) parameter estimates if the underlying assumptions concerning the model function and noise distribution are satisfied. VARPRO (*1*) and the more recent AMARES (*2*) are examples of these types of methods. On the other hand, statistically suboptimal black-box methods exist that are fully automatic (examples can be found in (*3–7*)). Minimal user interaction, a model function restricted to a sum of damped complex-valued sinusoids, and limited incorporation of prior knowledge are inherent to this type of models. Recent variants have been proposed in which some forms of prior knowledge can be imposed (*8–10*).

This paper focuses on interactive methods, since they are most often used in demanding *in vivo* applications. AMARES is selected here to represent this class of methods. The first part of the paper deals with the processing of a single MRS signal with AMARES.

Often, in time series of MRS signals additional information concerning the time evolution of the parameters is known. We show here that taking this available prior knowledge into account yields statistically better results than processing the signals separately. Optimal use of common information in a

1090-7807/99 $30.00

time series has been used previously for analysis of inversion-recovery data (*11*). In that case, a model function with an adjustable parameter for the time dependence was available. Here we account for common information in an optimal ML way without the availability of such a model function. In the second part of the paper, we explain how AMARES can be extended to the simultaneous processing of all spectra in the time series with imposition of prior knowledge on relations between different spectra in a ML setting. In the literature a suboptimal approach consisting of applying AMARES twice is sometimes used to analyze time series in case the common information among spectra consists of parameters which remain constant in time (*12*). We compare this with the ML approach. The methods presented are illustrated and tested using a Monte Carlo study on two different time series in the third section of the paper. Finally, we show the advantages of using the new optimal approach on an *in vivo* time series.

Note that in the frequency domain, analysis of series of spectra can be performed using principal component analysis (*13*). We also like to emphasize that the advantages of processing signals simultaneously using common information can be exploited in the frequency domain too. Model fitting methods in the frequency domain can be extended to the simultaneous processing of signals in exactly the same way as is done for AMARES. It is also possible to extend the black-box methods to the simultaneous processing of spectra. In (*14*) it is shown how this can be done. Although these algorithms do not perform as well in terms of precision as the extensions of interactive methods and still need some more fine tuning before they become really practical, they perform better than a black-box method applied on every signal individually and are promising black-box techniques to further automate the MRS data processing.

QUANTIFICATION OF A SINGLE MRS SIGNAL USING AMARES

In case the signal is modeled by Eq. [1], the following cost function has to be minimized with respect to the unknown amplitudes, dampings, frequencies, and phases in order to obtain ML estimates:

$$\sum_{n=0}^{N-1} \left| y_n - \sum_{k=1}^{K} a_k e^{j\phi_k} e^{(-d_k + j2\pi f_k)t_n} \right|^2 = \|\mathbf{y} - \Psi\mathbf{l}\|^2, \qquad [2]$$

with $\mathbf{y} = [y_0, \ldots, y_{N-1}]^T$ the signal vector, $\mathbf{l} = [a_1 e^{j\phi_1}, \ldots, a_K e^{j\phi_K}]^T$, and

$$\Psi = \begin{bmatrix} e^{(-d_1 + j2\pi f_1)t_0} & \cdots & e^{(-d_K + j2\pi f_K)t_0} \\ \vdots & \ddots & \vdots \\ e^{(-d_1 + j2\pi f_1)t_{N-1}} & \cdots & e^{(-d_K + j2\pi f_K)t_{N-1}} \end{bmatrix} \qquad [3]$$

is an $N \times K$ matrix of full rank; T denotes the transpose.

To perform the actual minimization the functional $\|\mathbf{y} - \Psi\mathbf{l}\|^2$ is split into a real and imaginary part and the resulting functional $\|\mathbf{y}^G - \Psi^G\mathbf{l}^G\|^2$ is minimized where

$$\Psi^G = \begin{bmatrix} e^{-d_1 t_0}\cos(2\pi f_1 t_0 + \phi_1) & \cdots & e^{-d_K t_0}\cos(2\pi f_K t_0 + \phi_K) \\ e^{-d_1 t_0}\sin(2\pi f_1 t_0 + \phi_1) & \cdots & e^{-d_K t_0}\sin(2\pi f_K t_0 + \phi_K) \\ \vdots & \ddots & \vdots \\ e^{-d_1 t_{N-1}}\cos(2\pi f_1 t_{N-1} + \phi_1) & \cdots & e^{-d_K t_{N-1}}\cos(2\pi f_K t_{N-1} + \phi_K) \\ e^{-d_1 t_{N-1}}\sin(2\pi f_1 t_{N-1} + \phi_1) & \cdots & e^{-d_K t_{N-1}}\sin(2\pi f_K t_{N-1} + \phi_K) \end{bmatrix}, \quad \mathbf{y}^G = \begin{bmatrix} \mathrm{Re}(y_0) \\ \mathrm{Im}(y_0) \\ \vdots \\ \mathrm{Re}(y_{N-1}) \\ \mathrm{Im}(y_{N-1}) \end{bmatrix}, \quad \mathbf{l}^G = \begin{bmatrix} a_1 \\ \vdots \\ a_K \end{bmatrix}. \qquad [4]$$

Re(.) and Im(.) denote the real and imaginary parts of a complex quantity, respectively, ||.|| denotes the Euclidean vector norm, and |.| denotes the modulus of a complex quantity.

AMARES uses a secant method *dn2gb* (the most recent version of NL2SOL, as recommended in (*15*)) to minimize the cost function. The Jacobian is calculated analytically. An advantage of using *dn2gb* is the fact that the algorithm allows the user to specify upper and lower bounds on the variables. We can use this feature to impose the natural bounds on the variables. The physical requirement of a positive damping can thus easily be imposed. Similarly, amplitudes, in the absence of *J*-modulation, cannot become negative, whereas the upper and lower bounds on the frequencies are determined by the spectral width. Phases can be constrained to lie in any range between $-180°$ and $+180°$. In general it is recommended to add those extra bounds on the variables in order to ensure maximum accuracy and robustness (*16*). AMARES allows the imposition of all kinds of linear relations between individual parameters.

The major problem with this nonlinear least-squares (NLLS) approach is the need for starting values for all unknowns. AMARES requires the user to provide starting values for frequencies and dampings. The starting values for the amplitudes and phases are obtained by solving the least-squares problem $\mathbf{y} = \Psi\mathbf{l}$, with the starting values for the frequencies

and dampings inserted in Ψ. The starting values for the frequencies and dampings are usually obtained by "peak-picking" on the FT of the signal. Note that AMARES can accommodate any model function and is therefore not restricted to exponentially damped sinusoids.

The full description of AMARES, including the detailed description of all the different forms of prior knowledge that can be imposed, is found in (*2*). The usefulness of AMARES in demanding *in vivo* applications is illustrated in (*17, 18*). AMARES is implemented within the software package MRUI (*19, 20*), a graphical user interface to facilitate the use of sophisticated analysis routines for MRS data quantification in biomedical/biochemical laboratories and the clinical environment.

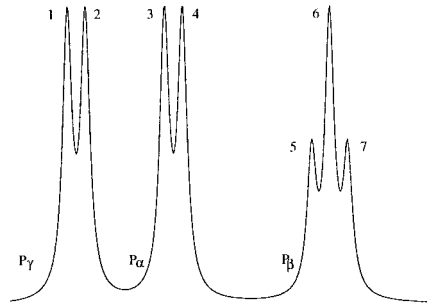

FIG. 1. Theoretical ^{31}P spectrum of adenosine triphosphate (ATP).

EXTENSIONS OF AMARES TO QUANTITATE TIME SERIES

ML Use of Common Information Present in Spectra: AMARES$_{ts}$

The quantification of time series can be formulated in a mathematical way as follows. Suppose we have S signals, each of which can be modeled by Eq. [1]. The nth sample of signal s, y_{ns}, is then given by

$$y_{ns} = \sum_{k=1}^{K_s} a_{ks} e^{j\phi_{ks}} e^{(-d_{ks}+j2\pi f_{ks})t_n}. \qquad [5]$$

The additional parameter index s indicates that the parameter refers to the sth signal of the time series and K_s denotes the number of peaks present in the sth signal. ML fitting of time series with relations between spectra boils down to minimizing the cost function

$$\sum_{s=1}^{S}\sum_{n=0}^{N-1} \left| y_{ns} - \sum_{k=1}^{K_s} a_{ks} e^{j\phi_{ks}} e^{(-d_{ks}+j2\pi f_{ks})t_n} \right|^2 = \|\mathbf{y}_{\text{series}} - \Psi_{\text{series}}\mathbf{l}_{\text{series}}\|^2, \qquad [6]$$

where

The relations present between spectra are expressed as relations between the corresponding parameters. In principle, any relation between parameters of the same type can be expressed. We describe shortly the possibilities currently implemented in this extension of AMARES, denoted by AMARES$_{ts}$ from now on. Each of the parameters can be left unconstrained or kept fixed. It is also possible to express a parameter as the sum of an unconstrained and a fixed parameter of the same type. Similarly, a parameter can be written as an unconstrained parameter of the same type multiplied with a fixed number. One can also express a variable as the sum of an unconstrained or a fixed parameter (of the same type), an unknown (and to be estimated) shift, and a fixed shift. An unknown (and to be estimated) ratio can also be used to express relations between parameters. Since the use of these unknown shifts or ratios leads to the introduction of a new variable, this new variable has to be shared by at least two parameters in order to reduce the total number of unknowns. We illustrate some of the prior knowledge that can be imposed using an arbitrary example of a time series consisting of two ^{31}P signals of the adenosine triphosphate (ATP) molecule. In Fig. 1 the spectrum of ATP obtained after Fourier transform is displayed. The P_α, P_γ resonances are split into two peaks (a doublet) and P_β is split into three peaks (a triplet) due to the J-coupling between the phosphorus nuclear spins in the ATP molecule. The prior knowledge available between the parameters of these seven

$$\mathbf{y}_{\text{series}} = [\mathbf{y}_1^T, \ldots, \mathbf{y}_S^T] = [y_{01}, \ldots, y_{(N-1)1}, \ldots, y_{0S}, \ldots, y_{(N-1)S}]^T,$$

$$\mathbf{l}_{\text{series}} = [\mathbf{l}_1^T, \ldots, \mathbf{l}_S^T] = [a_{11}e^{j\phi_{11}}, \ldots, a_{K1}e^{j\phi_{K1}}, \ldots, a_{1S}e^{j\phi_{1S}}, \ldots, a_{KS}e^{j\phi_{KS}}]^T,$$

$$\Psi_{\text{series}} = \begin{bmatrix} \Psi_1 & 0 & \cdots & \cdots & 0 \\ 0 & \ddots & & & 0 \\ \vdots & & \Psi_s & & \vdots \\ \vdots & & & \ddots & \vdots \\ 0 & \cdots & \cdots & & \Psi_S \end{bmatrix} \quad \text{with } \Psi_s = \begin{bmatrix} e^{(-d_{1s}+j2\pi f_{1s})t_0} & \cdots & e^{(-d_{Ks}+j2\pi f_{Ks})t_0} \\ \vdots & \ddots & \vdots \\ e^{(-d_{1s}+j2\pi f_{1s})t_{N-1}} & \cdots & e^{(-d_{Ks}+j2\pi f_{Ks})t_{N-1}} \end{bmatrix}.$$

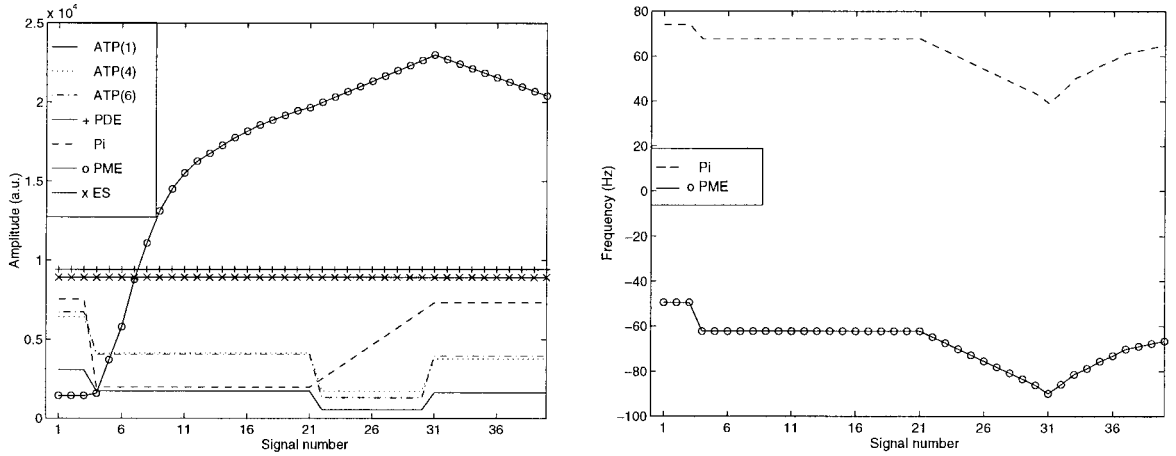

FIG. 2. Time variation of the parameters used in Example A. Left: amplitude variation of an external standard (ES), phosphomonoesters (PME), inorganic phosphate (P_i), phosphodiesters (PDE), and adenosine triphosphate (α-, β-, and γ-ATP) as a function of time (signal number). The number in parentheses in the ATP multiplets refer to the peak number as defined in Fig. 1. Right: frequency variation of P_i and PME as a function of time (signal number).

peaks within one signal can, e.g., be expressed as follows for every signal in the time series, $s = 1, 2$:

1. $a_{2s} = a_{1s}$, $a_{4s} = a_{3s}$, $a_{6s} = 2a_{5s}$, $a_{7s} = a_{5s}$; a_{1s}, a_{3s}, and a_{5s} are unconstrained, the other amplitudes are linked to them by a fixed ratio (1 or 2).
2. $d_{2s} = d_{1s}, \ldots, d_{7s} = d_{1s}$; d_{1s} is unconstrained and the other dampings are linked to it by a fixed ratio of 1.
3. $f_{2s} = f_{1s} - \Delta_{\text{fixed}}$, $f_{4s} = f_{3s} - \Delta_{\text{fixed}}$, $f_{6s} = f_{5s} - \Delta_{\text{fixed}}$, $f_{7s} = f_{5s} - 2\Delta_{\text{fixed}}$; $\Delta_{\text{fixed}} = 16$ Hz; f_{1s}, f_{3s}, and f_{5s} are unconstrained and the other frequencies are linked to them by the fixed shift Δ_{fixed}.
4. $\phi_{2s} = \phi_{1s}, \ldots, \phi_{7s} = \phi_{1s}$; ϕ_{1s} is unconstrained and the other phases are linked to it using a fixed ratio of 1.

Suppose now, that due to a change in the field homogeneity after the measurement of the first signal (see also Numerical Validation, Example B), an unknown increase in damping Δ_{var1} and an unknown shift in frequency Δ_{var2} occur for all peaks.

The prior knowledge for the dampings and frequencies of the peaks of the second signal must be changed to the following in order to express this extra information:

1. $d_{12} = d_{11} + \Delta_{\text{var1}}, \ldots, d_{72} = d_{11} + \Delta_{\text{var1}}$; $d_{12}, \ldots, d_{72}$ are linked to the unconstrained parameter d_{11} by introduction of a new variable Δ_{var1}, the unknown shift in damping.
2. $f_{12} = f_{11} + \Delta_{\text{var2}}$, $f_{22} = f_{11} - \Delta_{\text{fixed}} + \Delta_{\text{var2}}, \ldots, f_{72} = f_{51} - 2\Delta_{\text{fixed}} + \Delta_{\text{var2}}$; f_{12} and f_{22} are linked to f_{11}; f_{32} and f_{42} are linked to f_{31}, and f_{52}, f_{62}, and f_{72} are linked to f_{51} by a fixed shift Δ_{fixed} and by the unknown shift in frequency Δ_{var2}.

The prior knowledge we impose is a set of linear relations between parameters and as a consequence we obtain a minimization problem with linear equality constraints which we substitute

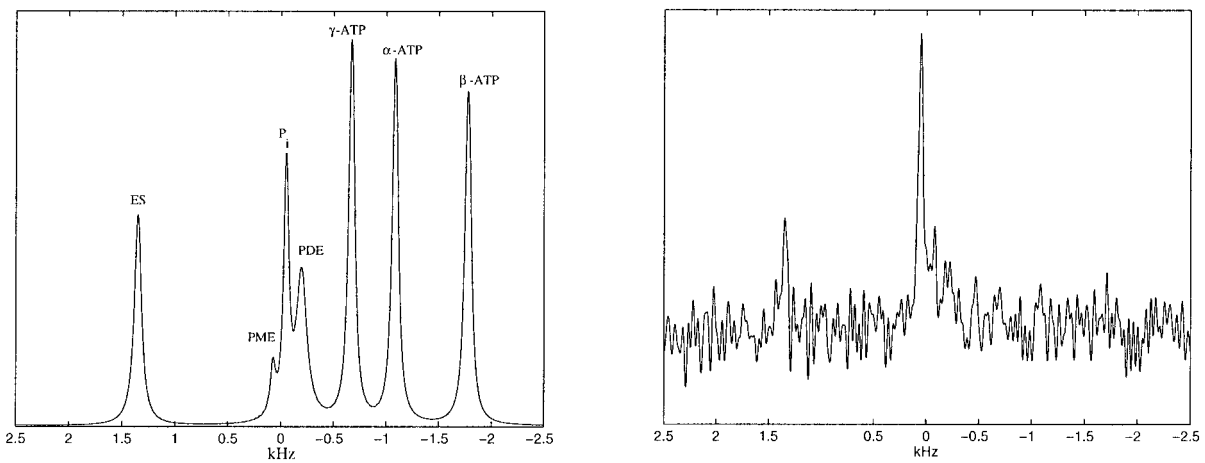

FIG. 3. Left: first signal of time series used in Example A without noise. Right: noisy realization ($\sigma_\nu = 3500$) of signal number 22.

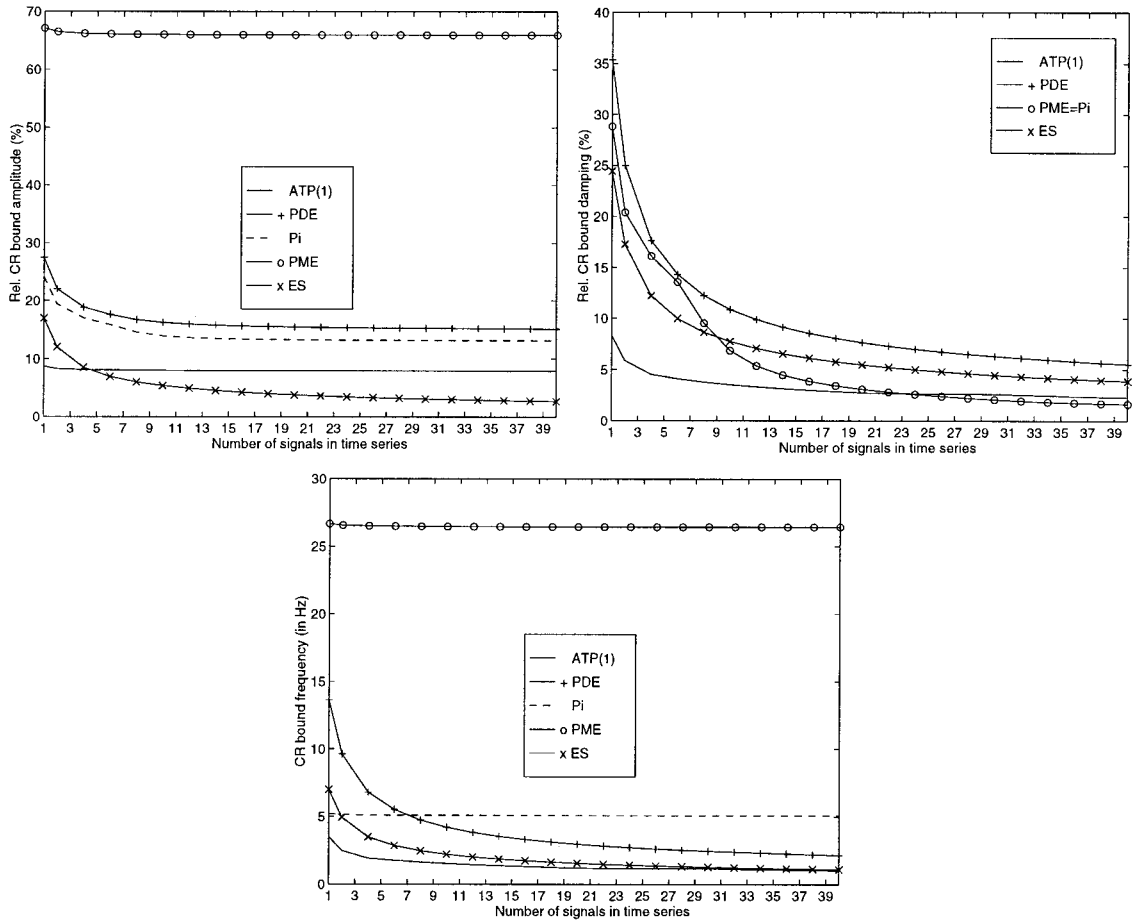

FIG. 4. (Rel) CR bounds (calculated at $\sigma_v = 3500$) of amplitudes, dampings, and frequencies of ATP(1), PDE, P_i, PME, and ES of the first signal in the time series of Example A are shown as a function of the number of consecutive signals of the time series that are processed simultaneously.

in the original functional in order to get an unconstrained NLLS problem. Currently the user has the choice between a Lorentzian or Gaussian model function for every peak.

The simultaneous processing of multiple signals of the time series increases the complexity of the optimization problem since the number of unknowns becomes larger. The needed storage for the Jacobian increases dramatically. Alternative optimization routines to alleviate these problems do exist. Large scale methods (e.g., LANCELOT (*21*), VE10 (*22*)) for solving large-scale nonlinear least-squares problems, exploit the so-called group partially separable structure of the nonlinear least-squares problem. The exploitation of the latter structure allows for efficient storage and calculation of gradients and Hessians (*23*). We are aware of these possible improvements, but since our main interest is the statistical properties of the proposed method, we still use *dn2gb* to minimize this cost function. This means that here also the Jacobian is calculated analytically and that upper and lower bounds on the variables can be imposed (see also the previous section). To perform the actual minimization, Ψ_s, $\mathbf{l}_s$, and $\mathbf{y}_s$, $s = 1, \ldots, S$ are split into a real and imaginary part as in Eq. [4]. The starting values for the amplitudes and phases are obtained by solving $\mathbf{y}_s = \Psi_s \mathbf{l}_s$, $s = 1, \ldots, S$, with the starting values for the frequencies and dampings inserted in Ψ_s, $s = 1, \ldots, S$.

Note that analyzing the signals in one round is only useful when information on relations between different signals is present. The newly developed method AMARES_{ts} will be incorporated in a future release of the MRUI package.

Suboptimal Use of Common Information Present in Spectra: $AMARES_{sts}$

An alternative to AMARES_{ts}, denoted here by AMARES_{sts}, that can be used to analyze time series in those cases where some of the parameters remain constant in time, has been described in the literature (*12*). The method proceeds as follows. In a first round every signal of the time series is analyzed separately using AMARES. Mean values of all the parameters known to remain constant in time are computed. Then an additional AMARES run is performed on every signal with these parameters fixed to the mean value found, in order to obtain more accurate parameter estimates for the time-varying

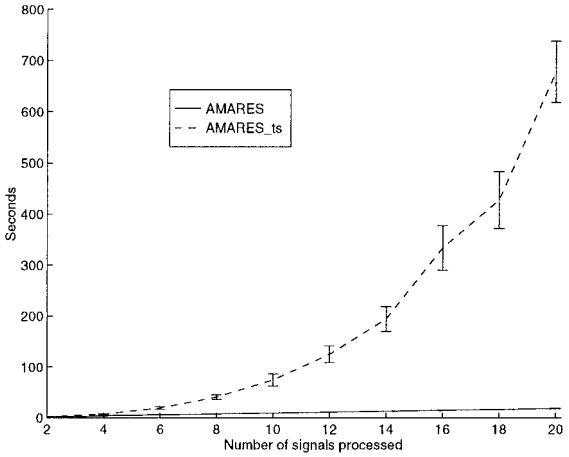

FIG. 5. Mean value and standard deviation (denoted by the error bars) of the CPU time in seconds needed by AMARES and $\text{AMARES}_{\text{ts}}$ as a function of the number of signals processed simultaneously (Example A).

parameters. This procedure leads to ML estimates as $S \rightarrow \infty$. Since only a limited number of signals are used to calculate the mean values, this approach may lead to biased estimates.

One could think of ways to extend $\text{AMARES}_{\text{sts}}$ to processing series of signals in which other types of time information are present, but the application of $\text{AMARES}_{\text{sts}}$ is less straightforward and more ad hoc in those cases and will not be pursued here.

NUMERICAL VALIDATION

In this section the methods presented are evaluated using Monte Carlo studies on two typical time series derived from experimental data.

TABLE 1

Failure Rates in Percent for Different Methods Used on Four Consecutive Time Frames Consisting of 10 Signals Each as a Function of the Noise Level σ_ν

σ_ν	Method	Frame 1	Frame 2	Frame 3	Frame 4
1000	AMARES	0	0	0	0
	$\text{AMARES}_{\text{sts}}$	0	0	0	0
	$\text{AMARES}_{\text{ts}}$	0	0.25	0	0
1500	AMARES	0.75	0	0.25	0
	$\text{AMARES}_{\text{sts}}$	1	0	0	0
	$\text{AMARES}_{\text{ts}}$	0	0	0	0
2000	AMARES	7.75	0.5	6.25	1.25
	$\text{AMARES}_{\text{sts}}$	5.75	0.5	0	0
	$\text{AMARES}_{\text{ts}}$	4.75	0	1	0
2500	AMARES	27.5	12.25	30.25	9.75
	$\text{AMARES}_{\text{sts}}$	18.75	8	4.5	0
	$\text{AMARES}_{\text{ts}}$	19.5	6.25	3.75	0
3000	AMARES	57	26.5	55.25	21.5
	$\text{AMARES}_{\text{sts}}$	30.5	21.75	22.75	0.25
	$\text{AMARES}_{\text{ts}}$	41	25.25	21.25	0.5
3500	AMARES	78	59	84.25	43.75
	$\text{AMARES}_{\text{sts}}$	49.75	42.25	41	2.5
	$\text{AMARES}_{\text{ts}}$	60.75	41	39.5	2

Note. Used methods: AMARES applied to every signal separately, $\text{AMARES}_{\text{sts}}$, and $\text{AMARES}_{\text{ts}}$.

In all examples each of the signals is modeled exactly by Eq. [1]. Statistical parameters like the (relative) root-mean-squared error (RMSE) are computed from the estimated parameters (using 400 runs), excluding parameters belonging to signals on which the method fails. A failure or bad run occurs if not all peaks are resolved within specified intervals lying symmetrically around the exact frequencies. The calculated RMSE are compared to the theoretical Cramér-Rao (CR) bounds, which

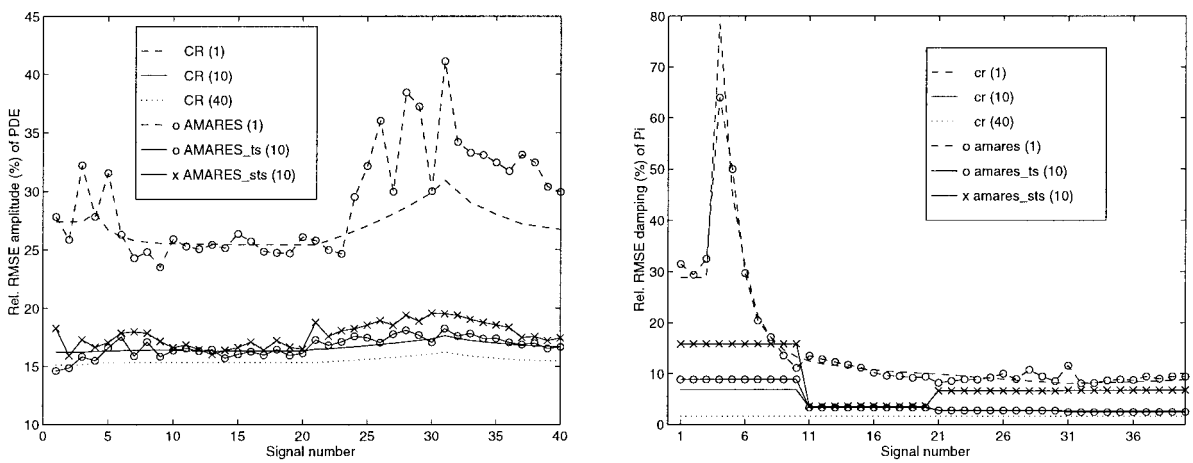

FIG. 6. Comparison of methods on the time series of Example A. Left: Rel RMSE ($\sigma_\nu = 3500$) of the amplitude of PDE as a function of time (signal number) obtained by AMARES applied separately to each signal, $\text{AMARES}_{\text{sts}}$ (four frames of 10 signals), and $\text{AMARES}_{\text{ts}}$ (four frames of 10 signals). Right: Rel RMSE ($\sigma_\nu = 3500$) of the damping of P_i as a function of time (signal number) obtained by AMARES applied separately to each signal, $\text{AMARES}_{\text{sts}}$ (four frames of 10 signals), and $\text{AMARES}_{\text{ts}}$ (four frames of 10 signals). Theoretical CR bounds are also depicted and denoted by CR. The number in brackets indicates the number of signals that is processed simultaneously.

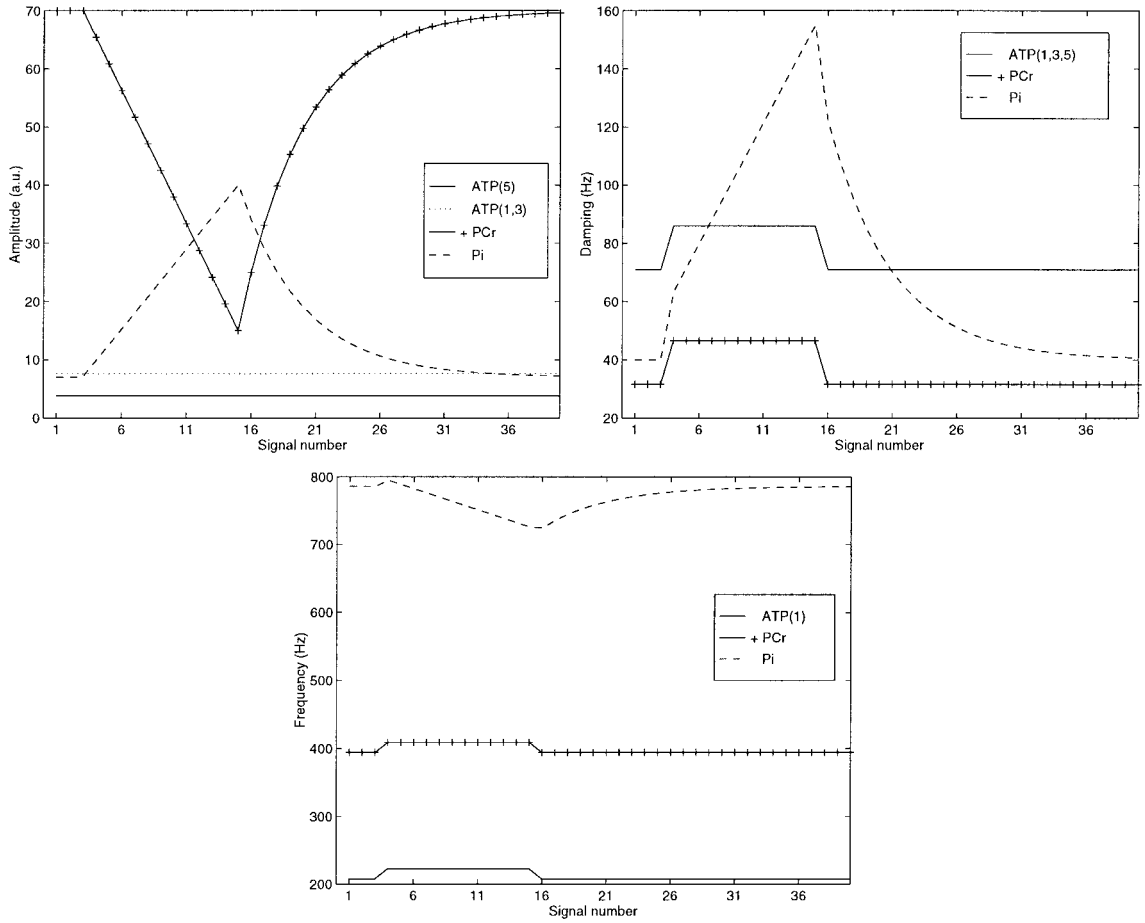

FIG. 7. Time variation of the parameters used in Example B. Top left: amplitude variation of inorganic phosphate (P_i), phosphocreatine (PCr), and adenosine triphosphate (α-, β-, and γ-ATP) as a function of time (signal number). Top right: damping variation of P_i, PCr, and ATP (α-, β-, and γ-ATP) as a function of time (signal number). Bottom: frequency variation of P_i, PCr, and γ-ATP (peak number 1 in Fig. 1; the variation of the frequencies of α- and β-ATP (not shown) is similar to that of γ-ATP) as a function of time (signal number). The number in parentheses in the ATP multiplets refers to the peak number as defined in Fig. 1.

provide a lower bound on the standard deviation of an unbiased estimator.

Example A

Monte Carlo studies were performed on a series of 40 simulated signals, derived from 40 ^{31}P-signals of an *ex vivo* perfused rat liver, acquired consecutively during administration of the fructose analogue 2,5-anhydro-D-mannitol (aHMol) (signals 4–21), subsequent administration of potassium cyanide (signals 22 to 30), and removal of aHMol (signals 31 to 40) (*24*). The corresponding changes in the amplitude of the phosphomonoesters (PME) (in casu, aHMolP esters), inorganic phosphate (P_i), and ATP peaks and in the frequency of the PME and P_i peaks are shown in Fig. 2. Peak linewidths remain constant over the experiment. The experimental signals were recorded at 81.1 MHz (4.7 T Bruker Biospec) with a temporal resolution of 100 s. Each signal consists of 128 complex data points. The sampling interval is 0.2 ms, t_0 and ϕ_k, $k = 1, \ldots,$ K, are zero. In Fig. 3 we observe peaks from an external standard (ES), PME, P_i, phosphodiesters (PDE), and adenosine triphosphate (α-, β-, and γ-ATP). The left-hand side of Fig. 3 shows a noiseless version of the first signal in the time series.

Due to the line broadening, the frequency splitting between the ATP multiplets is not visible from Fig. 3 but it is present. Noise from a Gaussian distribution with standard deviation σ_ν is added to the signals. We use seven noise levels varying form $\sigma_\nu = 500$ to 3500 in steps of 500. This implies that the SNR for, e.g., the reference peak, expressed in decibel (dB) and defined as $20 \log(a/\sigma_\nu)$ ranges from 57.6 to 18.7 dB. One noisy realization ($\sigma_\nu = 3500$) is shown in Fig. 3. Noise levels of $\sigma_\nu = 2000$ or 2500 are typical for *in vivo* experiments. In all results based on AMARES the following prior knowledge is used:

1. Within a signal: ATP prior knowledge as explained in the subsection “ML use of common information present in spectra:

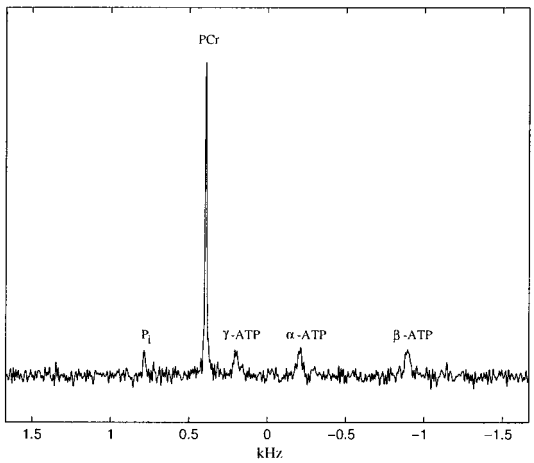

FIG. 8. Noisy realization ($\sigma_\nu = 5.2$) of the first signal of the time series used in Example B.

AMARES$_{ts}$", $\phi_k = 0$, $k = 1, \ldots, K$, $t_0 = 0$; damping of PME and P_i equal.

2. Between signals: the frequencies of ATP, PDE and ES, the dampings of all peaks, and the amplitude of ES remain constant.

This leads to the following number of parameters to be estimated: (6 *nr*signals + 1) unknown amplitudes, 4 unknown dampings, (2 *nr*signals + 5) frequencies; *nr*signals denotes the number of signals that is processed simultaneously. We obtained one set of starting values for the frequencies and dampings by peak-picking the first signal of the time series. These starting values were used for all the signals in the time series.

We have to choose how many signals will be analyzed simultaneously. There is a trade-off between accuracy and speed. On the one hand, results get more accurate as more signals are analyzed together. On the other hand, computer time and storage requirements increase. To gain some insight in this matter, we first analyze the possible improvements that can be made using the AMARES$_{ts}$ approach by looking at the theoretical CR bounds. We also perform a timing experiment. In Fig. 4 the (relative) CR bounds of the amplitude, damping, and frequency of the peaks of signal 1 are plotted versus the total number of signals that is processed simultaneously. The accuracy of parameters which are constrained to remain constant over time (i.e., the dampings of all peaks, the frequencies of all peaks except the ones of PME and P_i, and the amplitude of ES) increases substantially when more signals are processed simultaneously. The accuracy of the amplitudes of PDE and P_i is also increased significantly. Worth noting here is the fact that the accuracy of these peaks does not improve much further by processing more than about 10 signals at the same time.

Figure 5 shows the required CPU time (measured on a SUN ULTRA2 (200 MHz)). To process two signals individually with AMARES we need approximately 1.9 s, compared to 2 s with AMARES$_{ts}$. When every signal is analyzed separately using AMARES the required CPU time varies linearly with the number of signals processed. For AMARES$_{ts}$ the needed CPU time increases approximately cubically. For processing 20 signals at once 11 min are needed compared to 75 s when 10 signals are processed at once. Based on these observations concerning accuracy and required CPU time we divide our time series into four consecutive time frames each of 10 signals (so frame 1 consists of signals 1 to 10 of the time series, frame 2 is made up of signals 11 to 20, and so on).

On each of these frames we compare three methods in the Monte Carlo study: AMARES on each signal separately, AMARES$_{ts}$, and AMARES$_{sts}$.

In Table 1 the number of times one of these three algorithms

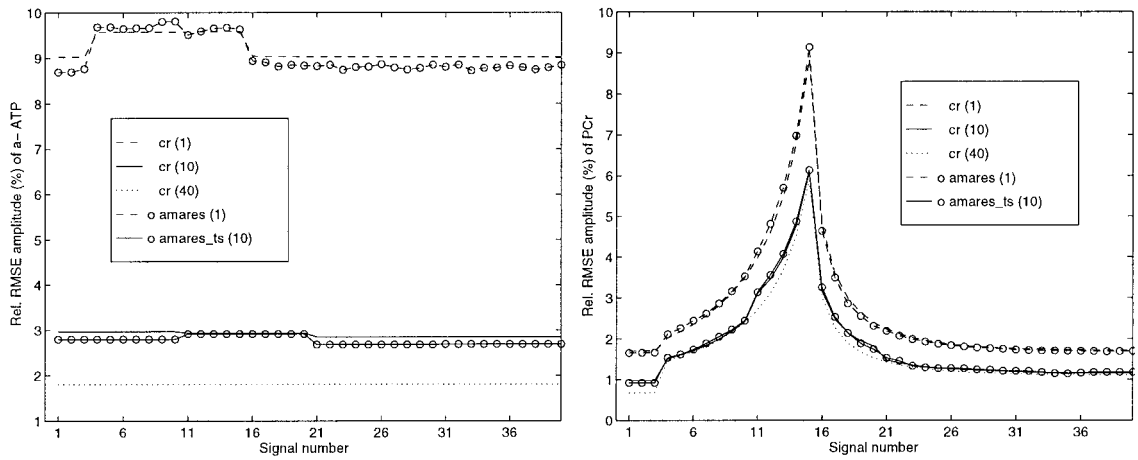

FIG. 9. Comparison of methods on the time series of Example B. Left: Rel RMSE ($\sigma_\nu = 5.2$) of the amplitude of the α-ATP peaks as a function of time (signal number) obtained by AMARES applied separately to each signal and AMARES$_{ts}$ (four frames of 10 signals). Right: Rel RMSE ($\sigma_\nu = 5.2$) of the amplitude of PCr as a function of time (signal number) obtained by AMARES applied separately to each signal and AMARES$_{ts}$ (four frames of 10 signals). Theoretical CR bounds are also depicted and denoted by CR. The number in parentheses indicates the number of signals that is processed simultaneously.

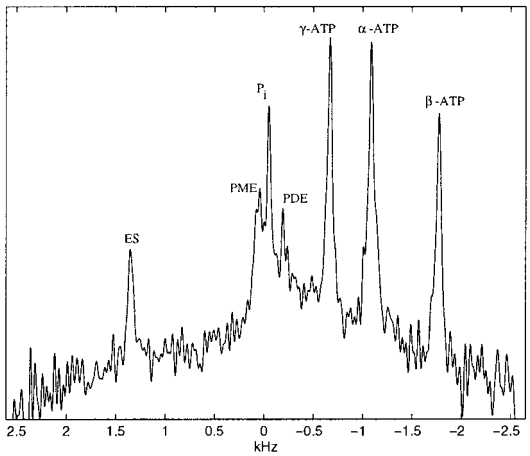

FIG. 10. *Ex vivo* ^{31}P signal from the perfused rat liver. On this figure, peaks from an external standard (ES), phosphomonoesters (PME), inorganic phosphate (P_i), phosphodiesters (PDE), and adenosine triphosphate (α-, β-, and γ-ATP) can be observed. The broad resonance underlying the mentioned metabolites originates from phosphorous nuclei in less mobile molecules. In the time domain we truncate the first data points to reduce its influence on the parameter estimates of the peaks of interest.

fails on the four different time frames as a function of the noise standard deviation is shown. We see that both $AMARES_{ts}$ and $AMARES_{sts}$ have a lower failure rate than AMARES applied to every signal individually.

On the left-hand side of Fig. 6 we compare the three methods in terms of the accuracy of the amplitude of PDE for the different signals in the time series ($\sigma_\nu = 3500$). The methods are compared to the theoretical CR bounds. In Fig. 6 three different CR bounds are plotted, one corresponding to the analysis of each signal separately, one corresponding to analyzing the signals simultaneously in sets of 10 signals, and one which shows the accuracy that can be obtained when the 40 signals are processed together. We again see that we do not lose much accuracy by splitting up the time series in four frames of 10 signals. AMARES and $AMARES_{ts}$ lie close to the corresponding CR bounds. Note that the erratic behavior of AMARES in time frames 1 and 3 is due to the fact that the failure rate of the method is very high (78 and 84.5%, respectively) in these frames and that the Rel RMSE shown is computed over a limited amount of successful runs. The erratic behavior disappears for lower noise levels. When we compare $AMARES_{ts}$ and $AMARES_{sts}$ for all the parameters we see that the first follows the CR bounds more closely. As an example of this we show on the right-hand side of Fig. 6 the Rel RMSE of the damping of P_i as a function of time. In time frames 1, 3, and 4, the estimates for the damping of P_i are farther away from the CR bound than the estimates obtained by $AMARES_{ts}$, which closely follow the CR bound. The gain in accuracy obtained by using $AMARES_{ts}$ is evident from these figures.

Example B

A Monte Carlo study is performed on a series of 40 simulated signals, derived from 40 *in vivo* ^{31}P signals of the calf muscle of a healthy human, acquired consecutively during an initial rest period (signals 1–3), an isometric contraction (signals 4–15), and the subsequent recovery period (signal 16–40). The experimental signals were acquired at 81.1 MHz (4.7 T Bruker Biospec) with a temporal resolution of 10 s, using a 5-cm-diameter surface coil positioned against the calf muscle. The corresponding changes in amplitude of the P_i and PCr peaks and of the frequency of the P_i peak are shown in Fig. 7. Also simulated is the often observed additional line broadening and frequency shift of all peaks during contraction, arising, e.g., from the altered B_0 homogeneity profile.

Each signal consists of 128 data points. The sampling interval is 0.3 ms, t_0 and ϕ_k, $k = 1, \ldots, K$, are zero. In Fig. 8 a noisy realization of the first signal of the simulated time series is displayed. Peaks from P_i, phosphocreatine, and adenosine triphosphate (α-, β-, and γ-ATP) can be observed. The standard deviation σ_ν used for the study is derived from the *in vivo* time series and is equal to 5.2. This corresponds to a SNR of 7.6 dB for the peaks in the α- and γ-ATP doublets.

For the ATP peaks the prior knowledge as described under Example A is used. The time dependencies imposed are the following:

1. The amplitudes of all the ATP peaks remain constant.
2. Dampings and frequencies of ATP and PCr remain constant for signals 1 to 3. In signal 4 the frequencies of PCr and ATP are shifted with a fixed unknown amount which remains constant throughout signal 15. Similarly, the dampings of PCr and ATP are increased from signal 4 throughout 15 with a fixed, unknown amount which remains constant. In signal 16 they return to their original values and remain constant throughout signal 40.
3. No temporal information is available for the P_i peak.

The prior knowledge can be taken into account by $AMARES_{ts}$ as explained under ML Use of Common Information Present in Spectra: $AMARES_{ts}$. The time series is again analyzed in four frames, consisting of 10 signals each. In this study we only compare AMARES and $AMARES_{ts}$ since there is no straightforward way to apply $AMARES_{sts}$ in this case. In Fig. 9 we compare the two methods in terms of the accuracy of the amplitude of α-ATP and PCr for the different signals in the time series. The methods are compared to the theoretical CR bounds. Three different CR bounds are plotted, one corresponding to the analysis of each signal separately, one corresponding to analyzing the signals simultaneously in sets of 10 signals, and one which shows the accuracy that can be obtained when the 40 signals are processed together. We again see that we do not lose much accuracy by splitting up the time series into four frames of 10 signals. AMARES and $AMARES_{ts}$ lie close to the corresponding CR bounds. The gains in accuracy

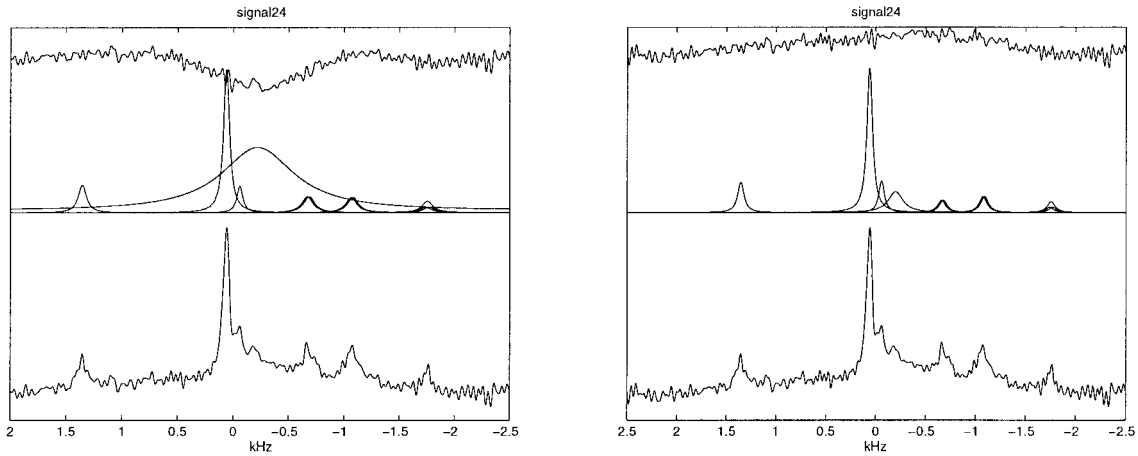

FIG. 11. Left: signal 24 of the time series fitted with AMARES. Right: signal 24 of the time series fitted with $\text{AMARES}_{\text{ts}}$.

obtained by applying $\text{AMARES}_{\text{ts}}$ are considerable for those peaks. For the P_i peak, for which no time information is present, there is no significant gain in amplitude accuracy (not shown). The gain in amplitude accuracy of the β- and γ-ATP peaks (not shown) is the same as for the α-ATP peaks.

In general, the gain in accuracy highly depends on the values and the time evolution of the parameters in the time series. For every specific case, however, it is possible to calculate the corresponding CR bounds, which gives an excellent indication of the gain in accuracy that can by obtained by using $\text{AMARES}_{\text{ts}}$.

EXPERIMENTAL TIME SERIES

We analyze here the experimental time series already described under Example A. An example of a signal of this time series is shown in Fig. 10.

In all the applied methods we omitted the first five data points to reduce the influence of the broad resonance underlying the metabolites of interest. We analyzed the 40 signals using AMARES applied on each signal individually. We imposed the same prior knowledge as under Example A; the phases and the begin time were fixed, and we imposed the ATP prior knowledge and constrained the dampings of PME and P_i to be equal. In 2 cases of 40 the algorithm failed to converge. In 3 other cases the PDE peak is obviously badly fitted. An example of such a bad fit is shown on the left-hand side of Fig. 11. We also fitted the time series with $\text{AMARES}_{\text{ts}}$ and we imposed in addition to the prior knowledge present within a signal that the frequencies of ATP, PDE, and ES, the dampings of all peaks, and the amplitude of ES remain constant over time. When we analyzed the signals using $\text{AMARES}_{\text{ts}}$ we encountered no convergence problems and all the signals were nicely fitted. On the right-hand side of Fig. 11 the corresponding successful $\text{AMARES}_{\text{ts}}$ fit of the signal badly fitted with AMARES is shown. When we use $\text{AMARES}_{\text{sts}}$ there are no convergence problems either. However, since this is an experimental signal there is no real objective way of drawing conclusions out of the small differences in fit obtained by $\text{AMARES}_{\text{ts}}$ and $\text{AMARES}_{\text{sts}}$.

CONCLUSIONS

Quantification of demanding *in vivo*, individual MRS spectra in the time domain is possible using interactive methods like AMARES. In this paper we present $\text{AMARES}_{\text{ts}}$, an extension of AMARES which allows us to take into account in a statistically optimal way the common information present in spectra of a time series. The method performs very well in practical situations. $\text{AMARES}_{\text{ts}}$ leads to improved and more robust estimates than the ones obtained by processing the signals individually with AMARES since in the latter case the information present between the spectra cannot be taken into account. It is also straightforward to extend the ideas used in the derivation of the $\text{AMARES}_{\text{ts}}$ algorithm to frequency domain fitting methods. The same concepts as explained in this paper can also be applied to MRSI. This is the subject of future research.

ACKNOWLEDGMENTS

The authors thank H.J.A. in 't Zandt of the Department of Radiology, University Hospital Nijmegen St. Radboud, for helpful discussions. LV is a Ph.D. student funded by the IWT (Flemish Institute for Support of Scientific–Technological Research in Industry). SVH is a Research Director with the F.W.O. (Fund for Scientific Research–Flanders). This work is supported by the Belgian Programme on Interuniversity Poles of Attraction (IUAP-4/2 and 24), initiated by the Belgian State, Prime Minister's Office for Science, Technology, and Culture, by the EU Programme "Training and Mobility of Researchers" project (contract ERBFMRXCT970160) entitled "Advanced Signal Processing for Medical Magnetic Resonance Imaging and Spectroscopy," by a Concerted Research Action (GOA) project of the Flemish Community, entitled "Model-Based Information Processing Systems," and by F.W.O. Grant G.0360.98.

REFERENCES

1. J. W. C. van der Veen, R. de Beer, P. R. Luyten, and D. van Ormondt, Accurate quantification of in vivo ^{31}P NMR signals using the variable projection method and prior knowledge, *Magn. Reson. Med.* **6,** 92–98 (1988).
2. L. Vanhamme, A. van den Boogaart, and S. Van Huffel, Improved method for accurate and efficient quantification of MRS data with use of prior knowledge, *J. Magn. Reson.* **129,** 35–43 (1997).
3. R. Kumaresan and D. Tufts, Estimating the parameters of exponentially damped sinusoids and pole-zero modeling in noise, *IEEE Trans. Accoustics Speech Signal Processing* **ASSP 30,** 833–840 (1982).
4. H. Barkhuysen, R. de Beer, W. M. M. J. Bovée, and D. van Ormondt, Retrieval of frequencies, amplitudes, damping factors, and phases from time-domain signals using a linear least-squares procedure, *J. Magn. Reson.* **61,** 465–481 (1985).
5. S. Y. Kung, K. S. Arun, and D. V. Bhaskar Rao, State-space and singular-value decomposition-based approximation methods for the harmonic retrieval problem, *J. Opt. Soc. Am.* **73,** 1799–1811 (1983).
6. S. Van Huffel, H. Chen, C. Decanniere, and P. Van Hecke, Algorithm for time-domain NMR data fitting based on total least squares, *J. Magn. Reson. A* **110,** 228–237 (1994).
7. Yuang-Ya Lin, P. Hodgkinson, M. Ernst, and A. Pines, A novel detection–estimation scheme for noisy NMR signals: Applications to delayed acquisition data, *J. Magn. Reson.* **128,** 30–41 (1997).
8. H. Chen, S. Van Huffel, D. van Ormondt, and R. de Beer, Parameter estimation with prior knowledge of known signal poles for the quantification of NMR spectroscopy data in the time domain, *J. Magn. Reson. A* **119,** 225–234 (1996).
9. H. Chen, S. Van Huffel, A. J. W. Van den Boom, and P. P. J. Van den Bosch, Subspace-based parameter estimation of exponentially damped sinosoids using prior knowledge of frequency and phase, *Signal Processing* **59,** 129–136 (1997).
10. S. Van Huffel, Subspace-based exponential data modeling using prior knowledge, *in* "Proceedings of the IEEE Benelux Chapter Signal Processing Symposium (IEEEBSPS)," pp. 211–214, Leuven, Belgium (1998).
11. D. van Ormondt, R. de Beer, A. J. H. Mariën, J. A. Den Hollander, P. R. Luyten, and J. W. A. H. Vermeulen, 2D approach to quantitation of inversion-recovery data, *J. Magn. Reson.* **88,** 652–659 (1990).
12. C. Decanniere, P. Van Hecke, F. Vanstapel, H. Chen, S. Van Huffel, C. van der Voort, B. van Tongeren, and D. van Ormondt, Evaluation of signal processing methods for the quantification of strongly overlapping peaks in ^{31}P NMR spectra, *J. Magn. Reson. B* **105,** 31–37 (1994).
13. A. C. Kuesel, R. Stoyanova, N. R. Aiken, Chun-Wei Li, B. S. Szwergold, C. Shaller, and T. R. Brown, Quantification of resonances in biological ^{31}P NMR spectra via principal component analysis: Potential and limitations, *NMR Biomed.* **9,** 93–104 (1996).
14. H. Chen, S. Van Huffel, A. J. W. Van den Boom, and P. Van den Bosch, Extended HTLS methods for parameter estimation of multiple data sets modeled as sums of exponentials, *in* "Proc. 13th Int. Conf. on Digital Signal Processing (DSP97)," pp. 1035–1038, Santorini, Greece (1997).
15. J. Dennis and R. Schnabel, "Numerical Methods for Unconstrained Optimisation and Nonlinear Equations," Prentice Hall, Englewood Cliffs, NJ (1983).
16. P. Gill, W. Murray, and M. Wright, "Practical Optimization," Academic Press, San Diego (1988).
17. A. van den Bergh, L. Vanhamme, S. Van Huffel, and A. Heerschap, Improving the SNR of glycogen detection in ^{13}C MRS by multiexponential signal fitting using prior knowledge, *in* "MAG*MA, Supplement to Volume V Number II (ESMRMB '97)," p. 190 (1997).
18. Š. Mierisová, A. van den Boogaart, P. V. H. I. Takáč, L. Vanhamme, V. Mlynárik, and T. Liptaj, New approach for quantitation of short echo time *in vivo* ^{1}H MR spectra of brain using AMARES, *NMR Biomed.* **11,** 32–39 (1998).
19. http://azur.univ-lyon1.fr/tmr/tmr.html.
20. http://www.mrui.uab.es/mrui/mruiHomePage.html.
21. A. Conn, N. Gould, and P. L. Toint, LANCELOT, "A Fortran Package for Large-Scale Nonlinear Optimization (Release A)," Series on Computational Mathematics 17, Springer-Verlag, Berlin (1992).
22. P. L. Toint, VE10AD: A routine for large-scale nonlinear least squares, *Harwell Subroutine Library* (1987).
23. P. L. Toint, On large-scale nonlinear least squares calculations, *SIAM J. Sci. Statist. Comput.* **8,** 416–435 (1987).
24. K. Bruynseels, N. Gillis, P. Van Hecke, W. Stalmans, and F. Vanstapel, Metabolic effects of the fructose analogue 2,5-anhydro-d-mannitol in perfused rat liver, *in* "Proceedings of the Society of Magnetic Resonance, Third Scientific Meeting," p. 1658, Nice, France (1995).